AGU PUBLICATIONS

JGR

Journal of Geophysical Research: Atmospheres

RESEARCH ARTICLE
10.1002/2015JD023961

Key Points:
- Tropical stratospheric upwelling is quantified using water vapor and carbon monoxide measurements
- Temporal variability in upwelling is dominated by the quasi-biennial oscillation and seasonal cycles

Correspondence to:
K. Minschwaner,
krm@nmt.edu

Citation:
Minschwaner, K., H. Su, and J. H. Jiang (2016), The upward branch of the Brewer-Dobson circulation quantified by tropical stratospheric water vapor and carbon monoxide measurements from the Aura Microwave Limb Sounder, *J. Geophys. Res. Atmos.*, *121*, 2790–2804, doi:10.1002/2015JD023961.

Received 18 JUL 2015
Accepted 14 FEB 2016
Accepted article online 18 FEB 2016
Published online 29 MAR 2016

The upward branch of the Brewer-Dobson circulation quantified by tropical stratospheric water vapor and carbon monoxide measurements from the Aura Microwave Limb Sounder

K. Minschwaner[1], H. Su[2], and J. H. Jiang[2]

[1]Department of Physics, New Mexico Institute of Mining and Technology, Socorro, New Mexico, USA, [2]Jet Propulsion Laboratory, California Institute of Technology, Pasadena, California, USA

Abstract The vertical distributions of water vapor (H_2O) and carbon monoxide (CO) in the tropical lower stratosphere are controlled largely by their mixing ratios near the tropopause and by ascending motions as part of the Brewer-Dobson circulation (BDC). The upward propagation of seasonal variations imprinted on H_2O and CO vertical profiles, often referred to as the tropical "tape recorder," can be used to derive the mean vertical velocity, $\overline{w^*}$, in this region of the lower stratosphere where quasi-horizontal mixing is not strong enough to erase the seasonal tape recorder signals. We used Aura Microwave Limb Sounder observations of the tropical tape recorders from 2004 to 2014 to derive values of $\overline{w^*}$ at pressures between 90 and 16 hPa (about 18 to 28 km altitude). Mean vertical profiles of $\overline{w^*}$ are consistent with calculated velocities derived from net radiative heating rates based on observed temperature, humidity, cloud, and trace gas amounts. Temporal variations in $\overline{w^*}$ are dominated by a quasi-biennial oscillation (QBO) and seasonal cycles, with maximum upwelling coinciding with easterly phases of the QBO in zonal wind shear and during the November–December period of the seasonal cycle. Both the QBO and annual modes emphasize the importance of wave phenomena in modulating the strength of tropical upwelling in the BDC. Interannual anomalies in $\overline{w^*}$ are correlated with variations in the El Niño–Southern Oscillation (ENSO), with enhanced stratospheric upwelling during El Niño phases and reduced upwelling during La Niña. A small decreasing linear trend (~6%/decade) in $\overline{w^*}$ is observed from 2005 to 2014, although confidence is low in identifying such a trend as part of a long-term change due to the influence of ENSO over this period.

1. Introduction

The dominant mode for the transport of chemical species throughout the stratosphere is the Brewer-Dobson circulation (BDC) [*Brewer*, 1949; *Dobson*, 1956], which is characterized by ascent at low latitudes, mean meridional motion in the upper stratosphere toward the poles, and descent at higher latitudes. Superimposed on this residual mean mass circulation, quasi-horizontal mixing within the extratropics [*McIntyre and Palmer*, 1984], and between the tropical and extratropical stratosphere [e.g., *Randel et al.*, 1993] can occur through a cascade of processes from planetary wave breaking to small-scale turbulent mixing [e.g., *Garny et al.*, 2014, and references therein]. In addition, the current picture of the residual circulation distinguishes between a deep branch between about 70 and 1 hPa, driven largely by waves in the middle and upper stratosphere, and a shallow branch between 100 and 70 hPa that is associated with wave breaking in the subtropical lower stratosphere [*Birner and Bönisch*, 2011; *Konopka et al.*, 2015]. The BDC exerts a major influence on the distributions of stratospheric compounds such as ozone (O_3), water vapor (H_2O), carbon monoxide (CO), methane (CH_4), nitrous oxide (N_2O) [e.g., *Solomon et al.*, 1986], and numerous other long-lived trace gases. Many of these compounds are important in regulating the penetration of solar ultraviolet radiation to the surface, or in the infrared greenhouse forcing of climate, or both [*World Meteorological Organization*, 2011]. Model simulations predict an intensification of the BDC associated with future climate change [*Butchart and Scaife*, 2001; *Austin and Li*, 2006]; thus, it is important to develop observational metrics for characterizing variability in the BDC.

One measure of the mean meridional mass circulation is the upward velocity of air in the low-latitude ascent region, which by mass continuity can be related to the entire circulation system. A related metric of the BDC is provided by the mean age of stratospheric air, defined as the average transit time of an air parcel since entering the stratosphere [e.g., *Waugh and Hall*, 2002]. Although neither the mean upwelling rate nor mean age is

amenable to direct measurement, both can be estimated from observations of long-lived compounds. In the case of mean age, quasi-passive tracers with monotonically increasing tropospheric concentrations, such as CO_2 or SF_6, can be used to estimate transit times [*Engel et al*., 2002]. For upwelling rates, the very slow velocities present a challenge for conventional meteorological measurement systems and the fact that the BDC is based on a Lagrangian framework that cannot be precisely quantified by Eulerian measurements. Wind-profiling Doppler radars have been used to observe monthly and seasonal mean vertical velocities in the upper troposphere and lower stratosphere [*Gage et al*., 1991; *Jagannadha Rao et al*., 2002, 2003], yielding values of 0.3 to 0.5 cm/s between 18 and 20 km altitude. Although the radar results are limited to single sites and therefore do not represent the true zonal mean upwelling rate, it should be noted that these measurements are up to a factor of 10 larger than those estimated by other techniques. *Rosenlof* [1995] calculated the transformed Eulerian-mean residual circulation using modeled heating rates constrained by data from the Upper Atmosphere Research Satellite and obtained mean upward velocities on the order of 0.01–0.03 cm/s at 70 hPa. *Randel et al*. [2002] derived velocities of similar magnitude using two methods: from thermodynamic constraints with calculated net radiative heating rates and from momentum balance and downward control [*Haynes et al*., 1991] applied to UK Meteorological Office (UKMO) analysis products. The latter method had been used previously by *Rosenlof and Holton* [1993], who also identified one of the difficulties associated with this approach arising from forcing by unresolved gravity wave drag.

Mote et al. [1996] examined the upward propagating signal in water vapor in the tropical lower stratosphere and used the term tape recorder to describe this phenomenon. They estimated upward speeds of 0.02 to 0.04 cm/s by following the time/height contours of variations in total hydrogen ($H_2O + 2{\cdot}CH_4$). Later studies [*Niwano et al*., 2003; *Schoeberl et al*., 2008; *Flury et al*., 2013] quantified the vertical velocities by calculating phase lags between trace gas anomalies at different pressure levels. *Schoeberl et al*. [2006] identified a similar tape recorder signal in stratospheric CO; they obtained good agreement with observations using a chemical transport model forced by climatological surface emissions of CO. Most recently, *Jiang et al*. [2015] compared vertical velocities derived from the H_2O tape recorder with results from meteorological reanalyses and found large differences in the data sets.

Here we describe a method for determining mean vertical velocities, with a time resolution of 3–4 months and an altitude resolution of ~2 km, by tracking the phase lag of tape recorder signals using Aura Microwave Limb Sounder (MLS) data.

2. Data Sets

We use version 3.3 Level 2 Aura MLS water vapor, carbon monoxide, and ozone products as described by *Read et al*. [2007], *Livesey et al*. [2008, 2011], and *Froidevaux et al*. [2008]. The MLS data have a vertical resolution of ~3 km for H_2O and O_3, and ~5 km for CO, and horizontal resolutions of ~7 km across-track and ~300 km along-track. The useful altitude ranges are at pressures $p \leq 316$ hPa for H_2O and $p \leq 215$ Pa for CO and O_3. The measurement uncertainties (including biases) for H_2O are 20% in the UT ($p > 100$ hPa) and 10% near the tropopause and in the stratosphere ($p \leq 100$ hPa); for MLS CO and O_3, the uncertainties are about 30%. We also used near-simultaneous measurements from the A-Train [*L'Ecuyer and Jiang*, 2010] instruments for inputs to the radiative transfer model used in the study [*Fu and Liou*, 1993]. These include vertical profiles of tropospheric and lower stratospheric temperatures and tropospheric H_2O from the Atmospheric Infrared Sounder (AIRS) [*Olsen et al*., 2007], upper tropospheric and stratospheric H_2O and O_3 profiles from MLS measurements, and cloud water content measurements by CloudSat [*Austin et al*., 2009] for $p > 215$ hPa and MLS ice water content for $p \leq 215$ Pa [*Wu et al*., 2008]. The uncertainties of AIRS data are ~25% for H_2O and 0.5 K for temperature. For cloud water content, the uncertainties are about a factor of 2, mostly due to uncertainties related to cloud particle size assumptions. For this study, the *McFarquhar and Heymsfield* [1997] ice crystal size parameterization is used. Where necessary, we interpolated all A-Train data onto the MLS footprint, as described by *Su et al*. [2009].

3. Methods

Figure 1 presents a conventional view of the H_2O and CO tropical tape recorder phenomena, where variations in tropical means are plotted as functions of pressure and time. In both cases, the temporal deviations in trace gas amounts are determined from the difference between measured, daily mean mixing ratios between 15°S

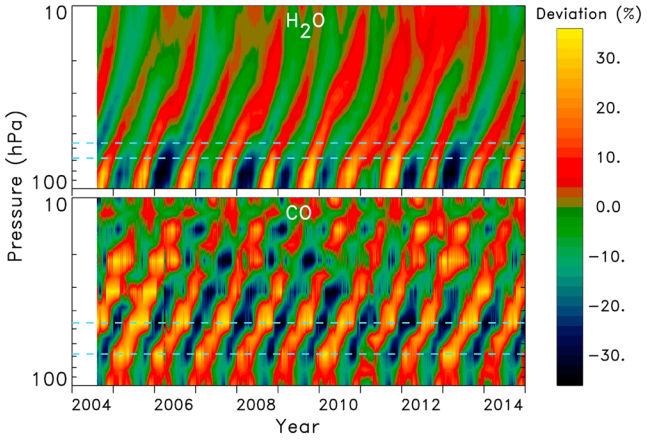

Figure 1. Tropical daily mean (15°S–15°N latitude) variations in mixing ratios of (top) H_2O, and (bottom) CO from MLS measurements, expressed as percent of the mean mixing ratio at each pressure level, for the time period from 8 August 2004 to 31 December 2014. Horizontal dashed lines denote pressure levels for the time series slices shown in Figure 2. The CO contours between pressure levels have been interpolated using a Fourier analysis for estimating the phase and amplitude [e.g., *Kim and Alexander*, 2013] of annual cycles between relatively coarse pressure coordinate grids for CO (6 per decade of pressure). This interpolation is not necessary for H_2O because the MLS H_2O measurements are made on a finer scale pressure grid (12 per decade).

and 15°N latitude, and the corresponding mean value over the full data period of ~10.4 years from August 2004 to December 2014. For H_2O, the tape recorder "head" is located near 100 hPa and it imparts an annual cycle with minima in January–February and maxima during July–August. For CO, the 100 hPa annual cycle is nearly reversed, with minima in August–September and pulses of maxima during the months of December through March. The vertical scale of the tape head for CO also appears to be larger than that for H_2O, and in many cases it extends above the 100 hPa level. This behavior might be related to a larger influence from deep convection in imprinting the CO signal [*Schoeberl et al.*, 2006], as opposed to variations in tropical tropopause temperature that are considered to be the main drivers for the H_2O signal [*Mote et al.*, 1996]. Alternatively, *Gettelman et al.* [2009] concluded that the annual cycle in lower stratospheric CO is governed primarily by variations in vertical velocity, and not convection. The coarser vertical resolution of CO measurements in comparison to H_2O could also play a role in apparent differences between tape heads. In any event, the details of the recording process appear to be considerably more complex for CO than for H_2O.

For both trace gases, the slopes of the upward propagating annual cycles can be used to estimate the ascent rate of within the tropical portion of the BDC. The chemical time constant for H_2O is very long (years) throughout the lower stratosphere [e.g., *Shimazaki*, 1985]. For CO, the photochemical lifetime is shorter (3–4 months) [e.g., *Ehhalt et al.*, 2007] but long enough to preserve the annual tape signal between MLS measurement levels. Thus, in the limit of no diffusive or eddy mixing, the derived ascent rates can provide a measure of $\overline{w^*}$, the vertical component of the residual mean meridional circulation [*Andrews et al.*, 1987]. This vertical velocity drives an important component of the thermodynamic equation

$$\frac{\partial T}{\partial t} + \overline{v^*}\,\overline{T}_y + \overline{w^*}\,\frac{H}{R}N^2 = \overline{Q}. \tag{1}$$

The first term represents the temperature tendency, the second term represents the mean meridional heat flux, and the third term represents mean heating from vertical motion. The term on the right side represents the mean diabatic heating rate, which is governed by the net longwave and shortwave radiative heating and cooling in the stratosphere. The notation otherwise follows that of *Andrews et al.* [1987].

As pointed out by *Schoeberl et al.* [2008], turbulent vertical mixing will reduce vertical gradients in the tape recorder signals and lead to an overestimate of $\overline{w^*}$; thus, vertical velocities derived from the tape signal should be regarded as upper limits to the residual mean vertical velocity. The net impact of quasi-horizontal mixing is more complicated. Extratropical trace gas abundances can be larger or smaller compared to tropical values and may contain seasonal variations that are not in phase with the tape recorder signals. Although the latter effect could be problematic in effecting the phasing of tropical tape recorder signals, we assume that these influences are small and that the most significant impact of eddy mixing into the tropical lower stratosphere is to decrease the amplitude of the tape signal [e.g., *Mote et al.*, 1998], with minimal impact on tape signal phases.

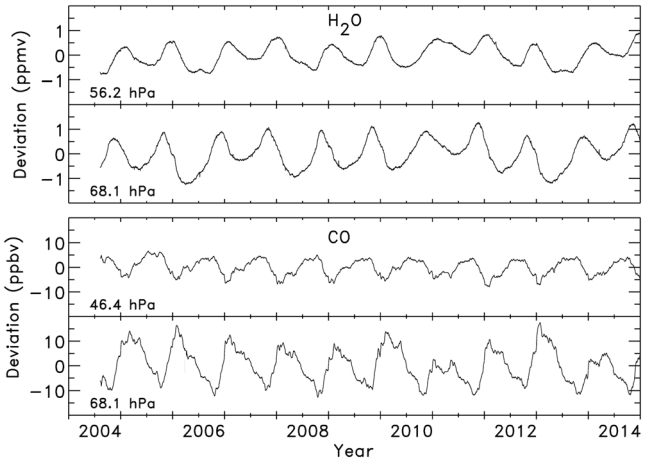

Figure 2. Time series slices of (top) H_2O and (bottom) CO tropical daily mean (15°S–15°N latitude) mixing ratio deviations from the overall mean at the indicated pressure. For each trace gas, adjacent pressure levels from MLS measurements are displayed; these are indicated by the dashed horizontal lines in Figure 1. The CO anomalies have been smoothed using a 7 day boxcar filter.

Time series of constant pressure "slices" through the tape recorder signals are shown in Figure 2 for pairs of adjacent measurement pressure levels, at 68.1 and 56.2 hPa for H_2O and at 68.1 and 46.4 hPa for CO. The annual cycles are clearly apparent in the time series for both gases, but variations in H_2O are more sinusoidal compared to those in CO, and consistent with the patterns shown in Figure 1; the CO annual maxima are punctuated by higher frequency variations lasting over 3–4 month periods. For both gases, the amplitudes of the annual cycles become smaller with decreasing pressure as the tape signal becomes diluted by the effects of mixing between the tropical and extratropical stratosphere [*Avallone and Prather*, 1996; *Minschwaner et al*., 1996]. Additionally for CO, photochemical production and loss reactions act to wash out the tape signal above about 30 hPa. The lower-pressure signals are phase lagged compared to those at higher pressure. Rough estimates of the phase lag are 2.5 to 3 months for H_2O and 4–6 months for CO, leading to a speed of $\overline{\omega} = \Delta p/\Delta t \approx 0.12$ to 0.18 hPa/day between these sets of pressure levels.

A more quantitative estimate of the phase lag can be made by applying harmonic analyses to determine phases of the annual cycles. Phase differences in the annual Fourier components over the full length of the time series shown in Figure 2 are 88 days for H_2O and 155 days for CO, yielding $\overline{\omega} = 0.135$ and 0.140 hPa/day, respectively. One advantage of the Fourier analysis is that it allows for interpolation between pressure levels for producing more coherent displays of the tape recorder, such as that shown for CO in Figure 1. A disadvantage is that the method requires multiple annual cycles which severely limits the time resolution of derived vertical speeds. In fact, there are significant annual and interannual variations in the phase lags that are large enough to be discerned by eye in Figure 2, but a Fourier decomposition can only provide a mean value.

The analysis here of the CO and H_2O tropical tape recorders generally follows earlier studies [*Niwano et al*., 2003; *Schoeberl et al*., 2008; *Flury et al*., 2013; *Jiang et al*., 2015], in which phase lags were determined between tape recorder signals at two pressure levels. Some of the details of our calculations, however, may differ from these previous studies. For each day and pressure level, we apply a fixed-width time window centered on that day to construct a truncated, weighted time series of the tape recorder signal. The time window employs a Hann weighting function [*Oppenheim et al*., 1999] to emphasize the signal near the center of the window and to reduce edge effects that can occur if no weighting is used. The Hann window, $w(n)$, is a symmetric function that is nonzero between $n = 0$ and $n = N$, where $N + 1$ is the full width of the window, and it has a maximum value of 1 at $n = N/2$. For the MLS data set, we found optimum full widths of $N = 365$ days for H_2O and $N = 475$ days (~1.3 years) for CO. The criteria used to select these values are discussed below.

Correlation coefficients are calculated between the truncated time series for a given day, and multiple time series constructed using the same Hann window on the adjacent (lower) pressure level, and centered over a range of time lags from 0 to 250 days. The sliding window date that produces the maximum correlation determines the inferred phase lag, calculated as the difference in time, dt, between the two pressure levels. In most cases, the maximum in the time series correlation as a function of phase lag was consistently found at phase lags between 20 and 200 days. The longest lag times were obtained for CO at the smallest vertical velocities (~0.1 hPa/day) and largest pressure differences between levels (~30 hPa for CO at the lowest levels). The pressure velocity $\overline{\omega} = \overline{dp/dt}$ is converted to a velocity in altitude coordinates, $\overline{\omega} = \overline{dz/dt}$, using tropical daily mean temperature profiles observed by MLS [*Schwartz et al*., 2008].

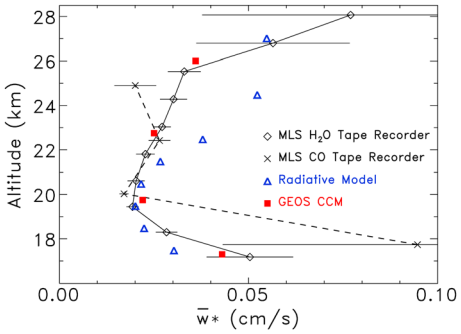

Figure 3. Vertical profiles of mean vertical velocity derived from MLS H_2O (diamonds, black solid curve) and MLS CO (X's, black dash curve) measurements. The time mean for MLS profiles covers the period from August 2004 to December 2014, and horizontal bars represent the standard deviation of daily values. Also shown are mean vertical velocities from radiative heating calculations (blue triangles) and from the GEOS climate chemistry model (red squares) [*Schoeberl et al.*, 2008].

Velocities calculated by this "sliced window correlation" method are mean values between two pressure levels and between two dates defined by the centers of the Hann windows [*Harris*, 1978]. The mean values were taken to be the actual velocities at the midpoint between pressure levels (in log(p)) and at a date determined by the mean of the center dates for the two windows. Sensitivity tests showed that a full width of 1 year for the Hann window was optimum for obtaining adequate signal and time resolution for H_2O. Values between 9 months and 15 months were tested; shorter time windows provided better time resolution but a poorer identification of the correlation maxima, leading to larger uncertainties in derived velocities. Longer time intervals produced higher signal/noise values but with poorer time resolution in vertical velocities. Similar sensitivity tests for CO showed that a slightly longer time window (1.3 years) was necessary due primarily to two factors, a larger pressure difference between measurement levels and a less sinusoidal tape signal at the tropopause. The latter behavior arises both from true geophysical variability in the tape signal and from generally higher noise in the CO measurements compared with H_2O. An additional complication arises in calculating optimum phase lags for CO due to the influence of photochemical production (primarily from methane oxidation) and loss (primarily from reaction with the hydroxyl radical), which both effect CO amounts on timescales comparable to the phase lag between measurement levels. Furthermore, methane and diurnal-mean hydroxyl both have seasonal variations in the tropical lower stratosphere, and the long stratospheric lifetime for methane may allow for a vertical propagation of methane seasonal cycles, which further complicates the traditional tape recorder view of CO variability. In contrast, the production of H_2O from CH_4 oxidation has a much smaller impact on phase lags computed from the H_2O tape signal because the timescale involved, $[H_2O]/P_{H2O}$, exceeds 1 year and is much longer than the phase lag between H_2O measurement levels.

Flury et al. [2013] used a similar sliced window correlation technique in an analysis of MLS tropical H_2O variations at 56 and 68 hPa. They derived a time series of $\overline{w^*}$ at 68 hPa for the period between 2005 and 2011 and found a strong quasi-biennial oscillation (QBO). The use of boxcar windows produced a limited time resolution (~1 year) so that annual variations in upwelling could not be retrieved. To obtain higher temporal resolution, *Niwano et al.* [2003] and *Flury et al.* [2013] used a dual profile correlation method, where optimum phase lags between partial vertical profiles were found, but velocities derived in this manner were vertically averaged over a larger range of altitude (~4–5 km).

Comparisons between application of the Hann window technique and a simple boxcar window showed that for equivalent window widths, the Hann weighting function consistently provided a more robust identification of the maximum in correlation as a function of time lag, as evaluated by the magnitude of the second derivative of the correlation function. Although this result did not lead to large differences in calculated velocities between the two approaches, it did lead to slightly lower error estimates for the Hann technique. A more significant advantage was gained in terms of effective time resolution. With a higher weighting near the center of the time window, the Hann method consistently provided an effective time resolution in vertical velocities that was at least a factor of 2 better than the boxcar window.

4. Derived Vertical Velocities

Figure 3 shows mean vertical profiles of $\overline{w^*}$ derived from the H_2O and CO tape recorders, along with their temporal variability. These profiles are based on the time means and standard deviations of daily values between 2004 and 2014. Mean velocities derived from H_2O and CO both show minima near 20 km altitude, and the magnitudes in this region agree well. However, at 18 km the CO-based value is a factor of 2 larger, and at 25 km it is about 30% smaller than the H_2O-based profile. At the lowest altitudes, the much faster

CO-based velocity is likely to be biased high by a closer proximity to the tape head (note that if two measurement levels actually span the tape head, then an infinite velocity would be obtained). At 25 km, the difference in derived mean velocities could be related to a systematic effect by CO production from methane oxidation.

In terms of variability, both velocity profiles indicate the highest temporal variability at the lowermost altitudes (25–50%) and at the highest altitudes (~30%), with much smaller variability (~10%) in the 19–22 km altitude region of minimum velocities. The higher values at the bottom and top of the velocity profiles are probably not entirely due to true geophysical variability because random uncertainties in daily velocities are become larger in these regions. Random uncertainties in daily values of $\overline{w^*}$ are about 10% for H_2O and 20% for CO in the 20–24 km region (see below), with larger uncertainties below 19 km and above 25 km. In addition, there are generally much larger random and systematic uncertainties in CO-based velocities due to the pressure gridding and signal variability issues discussed above. Systematic uncertainties for the means shown in Figure 3 are estimated at 3% for H_2O between 19 and 24 km, increasing to 5% at 17 km and 26 km. Systematic uncertainties for CO are 5% between 20 and 23 km, increasing to 8–10% at 18 and 25 km. For both gases, the systematic uncertainty is primarily related to the measurement accuracy and vertical variation in biases for low-latitude mixing ratios.

Our mean H_2O-based velocities are in good agreement ($<$10% differences) with values derived in the 20–24 km altitude region by *Niwano et al.* [2003] using Halogen Occultation Experiment (HALOE) observations and by *Flury et al.* [2013] from MLS observations. While it is not surprising that velocities compare well in the heart of the tape recorder region where uncertainties are generally lowest, we note that upwelling speeds at these altitudes are lower by 20–25% in comparison to values derived by *Schoeberl et al.* [2008] from HALOE and MLS data. At 18.7 km, there is a greater divergence of results between *Flury et al.* (0.020 cm s^{-1}), *Schoeberl et al.* (0.030 cm s^{-1}) and our H_20-based value (0.025 cm s^{-1}). At 26.4 km we find a large difference in velocities derived by *Flury et al.* and *Niwano et al.* (~0.031 cm s^{-1}) and the values from *Schoeberl et al.* and presented here (~0.05 cm^{-1}).

Figure 3 also shows mean velocities derived from the H_2O tape recorder simulated in a 30 year run using the Goddard Earth Observing System (GEOS) chemistry climate model [*Schoeberl et al.*, 2008]. We find good agreement between these simulations and our values from the observed MLS H_2O tape recorder. Although this result is generally consistent with the comparison by *Jiang et al.* [2015], they also found that standard reanalyses data sets tend to overestimate tape recorder derived $\overline{w^*}$, compared with MLS values, by factors of 2 or more below 20 km.

Vertical velocities can also be calculated using modeled net radiative rates and observed temperatures, assuming that the meridional heat flux and temperature tendency terms in equation (1) are relatively small [*Rosenlof*, 1995], so that

$$\overline{w^*} \approx \overline{Q}\left[\frac{\mathrm{d}\overline{T}}{\mathrm{d}z} + \Gamma\right]^{-1}, \tag{2}$$

where $\mathrm{d}T/\mathrm{d}z$ is the mean temperature lapse rate and $\Gamma = g/c_p$ is the dry adiabatic lapse rate [*Andrews*, 2010]. Figure 3 includes results based on net radiative heating rates calculated using the model of *Fu and Liou* [1993]. These were calculated for each day and averaged over a 4.5 year period between 2006 and 2010. The primary inputs to the radiative transfer calculations were collocated tropical, daily mean vertical profiles of AIRS tropospheric and lower stratospheric temperatures and tropospheric H_2O, MLS upper tropospheric and stratospheric H_2O and O_3, and cloud water content from measurements by the CloudSat and MLS, as in *Su et al.* [2009].

Agreement with the tape recorder velocities is very good around the region of minimum velocities at 20 km, but the radiatively based values are somewhat smaller at the lowest altitudes, and up to 50% larger near 24 km. Differences in this region could be related to difficulties in correctly simulating the shortwave heating by ozone. We carried out multiple radiative calculations with variable ozone inputs and found a high degree of sensitivity in calculated radiatively based velocities to the details of the ozone profile at these altitudes. It is important to note that positive, upward velocities are calculated using equation (2) because $\overline{Q}$ is positive in the tropical lower stratosphere (net radiative heating), and the net radiative term is composed of both longwave (both cooling and heating) and shortwave (heating) terms.

Daily variations in H_2O-based velocities over a 5 year period are displayed in Figures 4a and 4c, for pressures of 51.0 and 42.1 hPa, respectively. Also shown are daily values calculated using the radiative heating rates

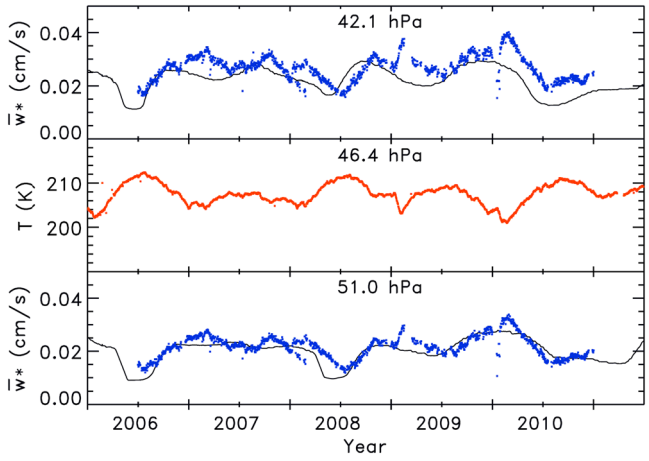

Figure 4. Black curves show time series of vertical velocities derived from the MLS H_2O tape recorder at (top) 42.1 hPa and (bottom) 51.0 hPa. Also shown in blue symbols are daily values of vertical velocity from radiative heating rate calculations. (middle) Red points show daily mean, tropical temperatures from MLS measurements at 46.4 hPa.

discussed above. At both pressure levels, temporal variations in vertical velocities track well. Higher frequency components (timescales less than ~month) components are seen in the radiatively based velocities compared to the tape recorder velocities, which are clearly low-pass filtered by the Hann window. The effective time resolution based on the widths of the narrowest features in the time series of H_2O-based velocities is between 3 and 4 months. Uncertainties in daily mean vertical velocities are controlled primarily by the sharpness of the correlation peak versus time lag between pressure levels, since the contribution from MLS measurement errors is much smaller in the tropical mean. Typically, the correlation maximum has an uncertainty of 2–5 days out of 20–50 days lag for H_2O; thus, uncertainties in daily mean velocities are on the order of 10%. The behavior of CO-based daily velocities are qualitatively similar to the ones from H_2O shown in Figure 4, but the time series from CO contain substantially more noise and are not used in the temporal analysis for section 4 below. As discussed above, a combination of various factors (larger measurement uncertainties, greater separation between measurement pressure levels, and chemical production/loss) render the CO tape recorder to be less reliable than the H_2O tape recorder for time series analysis.

A sensitivity analysis of the net radiative heating rates showed that calculated longwave heating and cooling at these levels are most impacted by the input vertical profiles of temperature and, to a lesser extent, water vapor and ozone (as noted above, ozone becomes increasingly important at lower pressures/higher altitudes). Tropospheric clouds have small but possibly important impact on both longwave and shortwave heating in the tropical lower stratosphere [e.g., *Dessler et al*., 1996]. Figure 4 includes the time series of daily mean tropical temperatures at 46.4 hPa. A strong anticorrelation between temperatures and radiative-based velocities is tied to the longwave emission rate: higher temperatures lead to increased longwave emission and associated radiative cooling, which reduces the net radiative heating rate. Variations in temperature displayed in Figure 4 can account for at least 65% of the variance in radiatively based velocities at both pressure levels shown. The equilibrium condition expressed by equation (2) requires that changes in $\overline{w^*}$ are accompanied by changes in net radiative heating, if changes in mean lapse rates are small. The current view of the mean meridional circulation emphasizes the importance of extratropical wave driving on upward velocities in the tropical lower stratosphere (the extratropical "suction pump") [e.g., *Holton et al*., 1995]. This extratropical forcing implies that temperature variations in the tropical lower stratosphere (or more precisely, departures from radiative equilibrium temperatures) result primarily from changes in $\overline{w^*}$ imposed from midlatitude and high-latitude planetary wave drag [e.g., *Randel et al*., 2002], although there remain questions about which waves are most important and the extent to which subtropical and tropical wave driving contributes significantly to tropical upwelling in the shallow branch of the BDC below 70 hPa [*Plumb and Eluszkiewicz*, 1999; *Kerr-Munslow and Norton*, 2006; *Randel et al*., 2008]. Changes in temperature are also related to quasi-biennial variations in tropical zonal winds [*Baldwin et al*., 2001, and references therein], which drive circulation anomalies that can be seen in vertical wind speeds, as discussed below.

5. Quasi-Biennial Oscillation, Annual Modes, and Interannual Variability

The QBO in the tropical stratosphere is characterized by alternating westerly and easterly zonal winds, with an approximate 2 year periodicity and downward propagation of wind phases [*Reed et al*., 1961], and an associated QBO in tropical stratospheric temperatures [*Angell and Korshover*, 1962]. There are numerous

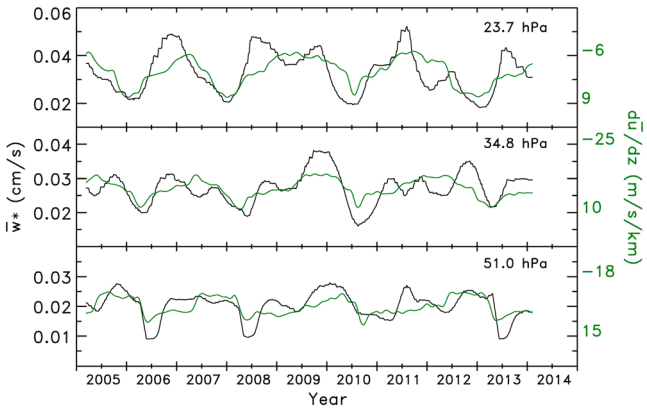

Figure 5. Time series of vertical velocity derived from MLS H_2O (black curves) at (top) 23.7 hPa, (middle) 34.8 hPa, and (bottom) 51 hPa pressure levels. Green curves at each pressure are zonal wind shears computed from monthly mean zonal winds over Singapore [*Naujokat*, 1986] and interpolated to daily values using cubic spline interpolation. Note the inverted axis for wind shear in order to more clearly display the anticorrelation with vertical velocity.

QBO-related phenomena occurring in the extratropics as well [e.g., *Bowman*, 1989; *Holton and Tan*, 1980], but the discussion here will focus on tropical QBO signals and their relationships to the ascending branch of the BDC.

One of the most complete and widely used records of the QBO is the monthly mean zonal wind time series from the Institute for Meteorology at Freie Universität Berlin (FUB), which is based on radiosonde observations from Singapore for the period from 1975 to present [*Naujokat*, 1986]. Figure 5 compares the wind shear calculated from FUB zonal mean winds, $\overline{u_z} = d\overline{u}/dz$, with daily mean vertical wind speeds calculated from the H_2O tape recorder at 51.0, 34.8, and 23.7 hPa. The period of record for vertical velocities is slightly less than 10 years due to the truncation of at least 6 months of data at both ends of the tape recorder time series from the Hann window analysis. Wind shears were calculated using tropical mean temperatures to transform pressure to altitude and then interpolated to the pressure grid used for vertical velocities. A final interpolation from monthly means to daily values was using done using cubic splines. This interpolation has a negligible impact on the correlation analysis below and is done primarily for visual interpretation in Figure 5.

Zonal wind shear and upward velocities are highly anticorrelated at the pressures shown in Figure 5. In addition to the inverted axis for used zonal wind shears to emphasize this anticorrelation, wind shear magnitudes have been scaled in Figure 5 to match the regression of wind shear and upward velocity time series at each level. There is a slight tendency for better tracking of the signals during positive wind shear phases (westerlies overlying easterlies), when mean upward velocities show distinct minima lasting only 2–3 months. In contrast, negative phases of wind shear are characterized by longer duration maxima in mean upward velocities. The close correspondence between $\overline{w^*}$ and $\overline{u_z}$ is consistent with QBO model simulations that show meridional circulation (BDC) anomalies imposed by thermal wind balance, with sinking anomalies (reduced ascent rates) in positive shear zones and rising anomalies (increased ascent rates) in negative shear zones [e.g., *Plumb and Bell*, 1982]. In addition, the QBO features observed in $\overline{w^*}$ propagate downward at a rate of 4–6 hPa/month (Figure 5), consistent with observations of the downward propagation speed of zonal mean wind regimes (~1 km/month) [*Wallace*, 1973] and as predicted from the theory of wave-mean flow interactions that drive the QBO [*Holton and Lindzen*, 1972]. Shorter durations of vertical velocity minima on constant pressure levels in Figure 5 are also consistent with observations showing that positive shear zones generally descend more rapidly than negative shear zones [e.g., *Naujokat*, 1986].

Signatures of the QBO have also been identified in $\overline{w^*}$ derived by *Niwano et al*. [2003] and *Flury et al*. [2013]. The former study found deseasonalized, interannual variations with amplitudes of 0.006 cm s^{-1} near 50 hPa increasing to 0.012 cm s^{-1} near 20 hPa, while the latter study found interannual variations of ±50% between 50 hPa and 20 hPa. Assuming that most of the interannual variability is dominated by QBO effects, these previous values are in reasonable agreement with the QBO amplitudes shown in Figure 5. In particular, we also find significant increases in QBO amplitudes with increasing altitude, as found by *Niwano et al*. [2003].

Although the QBO in zonal mean winds account for a large fraction of the temporal variability in $\overline{w^*}$, seasonal cycles are also found to be an important mode of variability. Annual components are more apparent after removing the QBO signal using a regression of the FUB zonal wind shear with the vertical velocity time series. Figure 6 shows vertical velocity, with the mean and QBO signals removed, at pressures of 61.8, 51.0, and 34.8 hPa. Also shown in Figure 6 are optimum fits for the phases and amplitudes of annual sinusoids at each

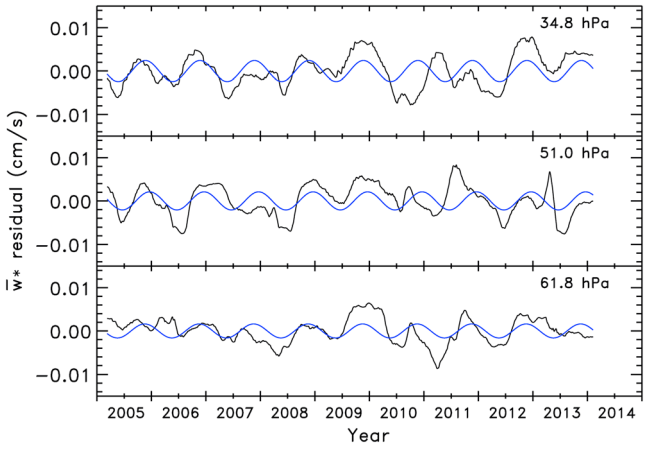

Figure 6. Time series of residuals in mean vertical velocities (black curves) at (top) 34.8 hPa, (middle) 51.0 hPa, and (bottom) 61.8 hPa, obtained by subtracting mean values and regressed QBO signals in wind shear from the FUB monthly mean zonal winds at Singapore [*Naujokat*, 1986]. Blue curves show optimal annual sinusoids with fitted phase and amplitude parameters.

level. Maxima in the annual components of vertical velocities were generally found during the months of November and December at all levels, with no significant changes in phase with altitude. As the effective time resolution of the H_2O tape recorder derived velocity is on the order of 3 months, it is unlikely that the phases of seasonal cycles can be determined with higher precision. Even so, the finding of maximum vertical velocities during November–December is consistent with results of radiative heating calculations constrained by assimilation model temperatures and measured trace gases [*Rosenlof*, 1995]. Seasonal amplitudes, however, appear to be smaller (~0.003 cm/s) in comparison to previous estimates (~0.01 cm/s) [e.g., *Randel et al*., 2002]. The limited temporal resolution (3–4 months) of our tape recorder derived velocities may be important here, as seasonal amplitudes are likely to be underestimated, particularly if they are not sinusoidal. The seasonal amplitudes shown in Figure 6 are in good agreement with the results of *Niwano et al*. [2003] at 61.8 and 52 hPa but are smaller by 50% at 34.8 hPa.

As discussed in section 1, current understanding of the annual cycle in the BDC above the 70 hPa level is that it is driven largely by seasonal variations in forcing from the dissipation of vertically propagating Rossby and gravity waves in the extratropical stratosphere [e.g., *Holton et al*., 1995]. The maximum in extratropical wave forcing in the Southern Hemisphere occurs roughly between September and November, whereas the forcing maximum in the Northern Hemisphere occurs roughly from November to March [*Randel et al*., 2002]; thus, the global wave forcing is largest during the September–March period, consistent with the seasonal maximum in $\overline{w^*}$ observed here. *Niwano et al*. [2003] found annual maxima during December–January, about a month later than the phase of our annual maxima. Although a comparatively precise seasonal phasing was not reported by *Flury et al*. [2013], they also identified annual maxima during Northern Hemisphere autumn and winter months.

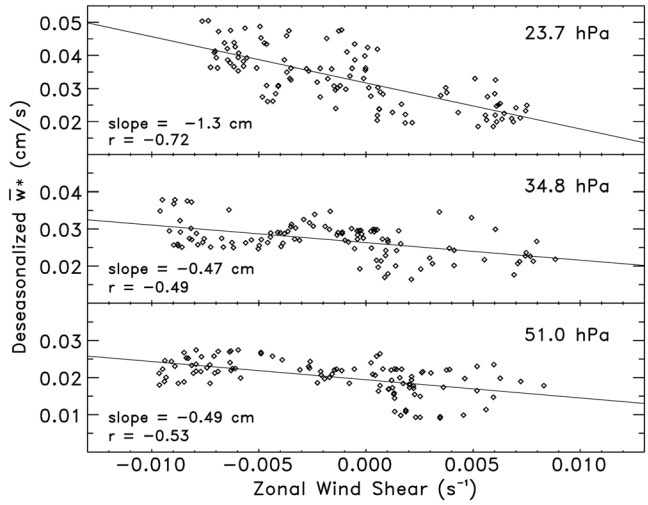

Figure 7. Scatterplot of deseasonalized vertical velocities versus zonal wind shear at (bottom) 51.0 hPa, (middle) 34.8 hPa, and (top) 23.7 hPa. Linear fits (solid lines) and slopes are indicated at each pressure level.

Identification of the annual phases and amplitudes also permits a closer examination of the relationships between vertical velocities and zonal wind shear. As noted above, these quantities are expected to be correlated due to the thermal wind relationship between zonal wind shear and temperature, and due to the influence of temperature on net radiative heating and vertical motion. Figure 7 shows scatterplots of deseasonalized, monthly mean $\overline{w^*}$ and $\overline{u_z}$ at three levels, along with least squares linear fits. We find significant levels of anticorrelation ($r < -0.5$) at all pressures between 60 and 20 hPa, with

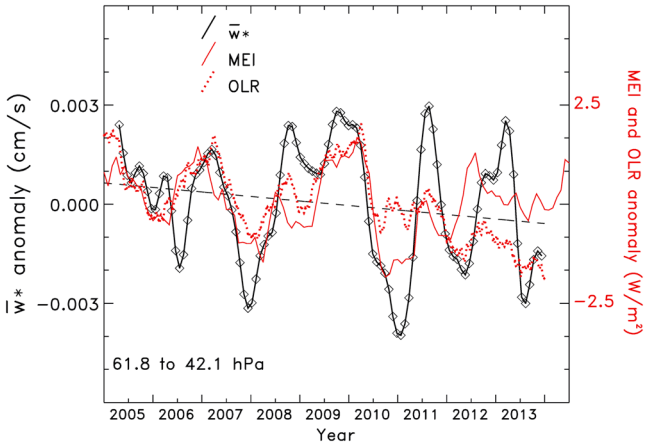

Figure 8. Residual, interannual anomaly in vertical velocity, averaged over three pressure levels between 61.8 and 42.1 hPa, and bin-averaged by month (black diamonds). The residuals were obtained by subtracting the fitted QBO and annual components from each vertical velocity time series. Red solid curve shows the Multivariate ENSO Index (MEI), and red dotted curve shows anomalies in tropical (15°S to 15°N) outgoing longwave radiation (OLR). The OLR anomalies were obtained by subtracting a fitted annual component to the tropical mean of gridded daily OLR measurements [*Liebmann and Smith*, 1996]. The velocity and OLR anomalies have been boxcar smoothed by 120 days, while the MEI represents 2 month mean values. Dashed black line indicates linear least squares fit to monthly vertical velocities.

slope magnitudes growing larger with decreasing pressure. *Randel et al.* [1999] obtained compact linear correlations using UK Meteorological Office (UKMO) assimilated winds and calculated values of $\overline{w^*}$ from UKMO temperature fields. The larger scatter seen in Figure 7, relative to the results of Randel et al., is likely due to other forms of geophysical variability in temperatures, radiative heating rates, and/or quasi-horizontal mixing that are projected onto $\overline{w^*}$. The range of slopes, $\delta\overline{w^*}/\delta\overline{u_z}$, is between −0.013 and −0.036 $(\mathrm{km\,mo^{-1}})/(\mathrm{m\,s^{-1}\,km^{-1}})$, which is on the low end of the value found by *Randel et al.* [1999] at 32 mb ($-0.033\ (\mathrm{km\,mo^{-1}})/(\mathrm{m\,s^{-1}\,km^{-1}})$). These differences should not be considered significant in light of the uncertainties in our analysis, along with consideration of the temperature anomaly correction employed by *Randel et al.* [1999], in which reanalysis QBO temperature anomalies were increased by a factor of 1.4 in order to better agree with observed temperature anomalies. However, we both find increasing slope magnitudes with height, consistent with the expectation that $\delta\overline{w^*}/\delta\overline{u_z}$ is inversely proportional to the radiative damping timescale [*Randel et al.*, 2002], which decreases with increasing altitude in the lower stratosphere [e.g., *Newman and Rosenfield*, 1997].

Additional variability in $\overline{w^*}$ that cannot be attributed to seasonal or QBO effects (as indicated in Figure 7) may be related to changes in the tropical stratosphere induced by El Niño–Southern Oscillation (ENSO). *Marsh and Garcia* [2007] found significant correlations between the Niño 3.4 index and modeled temperature, ozone, and upwelling in the tropical lower stratosphere, consistent with the propagation of ENSO signals into the stratosphere analyzed by *Garća-Herrera et al.* [2006] in general circulation model and reanalysis data sets. Figure 8 shows the time series of vertical wind speed anomalies with QBO and annual signals removed, averaged over three pressure levels from 61.8 to 32.1 hPa. These anomalies are significantly smaller than the amplitudes of QBO and annual modes seen on individual pressure levels, and therefore, an average was used to reduce noise in the time series. Figure 8 includes a time series of the Multivariate ENSO Index (MEI) [*Wolter and Timlin*, 2011]. The MEI is based on six observed variables over the tropical Pacific: sea-level pressure, zonal and meridional components of the surface wind, sea surface temperature, surface air temperature, and total cloudiness fraction of the sky. Although ENSO is primarily a tropospheric phenomenon with major impacts on tropical circulations, convective activity, and extratropical weather patterns, we find a strong correlation here ($r = 0.56$) with the rate of upwelling in the tropical lower stratosphere. Positive anomalies in vertical velocity correspond with El Niño phases (positive MEI) in 2006–2007 and 2009–2010, while negative anomalies in vertical velocity correspond with La Niña phases (negative MEI) in 2007–2008 and 2010–2011. In view of the global-scale tropospheric effects of ENSO, it is difficult to pinpoint mechanisms linking ENSO and the BDC. Modulation of wave driving by ENSO likely plays an important role, such as from planetary Rossby waves in the midlatitude Northern Hemisphere [*Garća-Herrera et al.*, 2006] or from orographic gravity waves in the Northern Hemisphere subtropics [*Calvo et al.*, 2010]. There may also be an important effect from changes in tropical convective activity due to ENSO. Deep convection is a major source for upward propagating gravity waves in the lower tropical stratosphere [e.g., *Jiang et al.*, 2004].

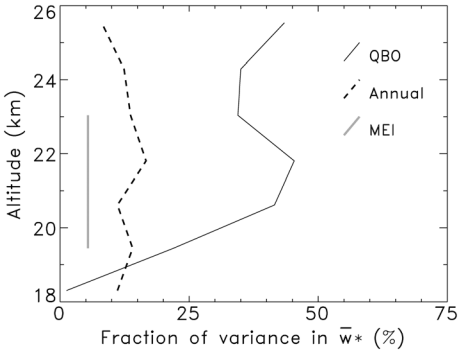

Figure 9. Fraction of the total variance, σ^2, in vertical velocity that is determined by the variance in regressed QBO (solid black), annual cycles (dashed black), and ENSO as gauged by the MEI (thick solid gray). In the case of annual cycles, the variance is estimated by $A^2/2$, where A is the amplitude of regressed sinusoidal functions.

Figure 8 also includes a time series of interannual anomalies in tropical mean, outgoing longwave radiation (OLR) [*Liebmann and Smith*, 1996]. These values are correlated with ENSO through modulation of the overall level of deep convective activity [e.g., *Su and Jiang*, 2013, and references therein]. Larger mean OLR corresponds to reduced overall convection in the tropics during El Niño, while smaller mean OLR is linked to enhanced tropical convection during La Niña. The positive correlation between vertical velocity and OLR anomalies is also robust ($r = 0.58$) and suggests a possible link to the dynamics of the tropical stratosphere through the longwave radiation field. In the absence of high clouds, longwave radiative heating in the lower stratosphere is enhanced due to absorption of upwelling radiation from the surface and lower troposphere in atmospheric "window" regions between 8 and 12 μm wavelengths [e.g., *Olaguer et al*., 1992]. Increasing fractions of high, cold cloud tops reduce longwave heating in the tropical lower stratosphere, and more than compensates for increased shortwave heating due to cloud albedo [*Fueglistaler and Fu*, 2006]. As the vertical velocity is directly related to the net radiative heating (equation (2)), this may partly explain the high correlation between ENSO and tropical mean upwelling in the tropics. One way to distinguish between wave-driven effects and cloud radiative effects on upwelling would be to compare time lags between ENSO and $\overline{w^*}$ anomalies. Modeled ENSO-related wave forcing produces a maximum response in upwelling during the El Niño phase, with a lag of 2–3 months [*Marsh and Garcia*, 2007; *Calvo et al*., 2010]. On the other hand, it might be expected that cloud radiative effects on net longwave heating would be more rapid, so that any effect on upwelling would therefore involve a much smaller response time. Unfortunately, we cannot distinguish phase lag response times at the monthly level given the limitations on temporal resolution (3–4 months) in the present analysis.

In addition to the interannual anomalies noted above, there is a small but statistically significant downward trend in the anomalies over this period from March 2005 to December 2013. The significance slightly exceeds the 95% confidence level, using a two-tailed t test for the null result on monthly mean anomalies shown in Figure 9. The slope of this trend corresponds to a decrease of 0.0014 cm/s/decade (−6%/decade), which is not significantly larger than the uncertainty (~0.0006 cm/s) in time mean velocities. Furthermore, this result is heavily influenced by the behavior near the beginning and end of the time period, which contain moderate El Niño and La Niña phases, respectively. If the regressed ENSO signal is removed, then the slope becomes smaller at −4%/decade and the significance is reduced such that a zero slope cannot be confidently ruled out.

In terms of the overall mass flux through the stratosphere, an implied 6% reduction in mean upwelling would suggest a similar decrease in mass flux if the dimensions of the large-scale circulation remain fixed. In the troposphere, quantification of any poleward expansion of the Earth's tropical regions is an area of active research [e.g., *Birner et al*., 2014, and references therein], and although several studies present evidence for increases in the width of the tropics of between 0.2° and 2.0° latitude/decade, results are highly sensitive to the metrics used to quantify the expansion rate [*Davis and Rosenlof*, 2012; *Davis and Birner*, 2013]. Note that an increase in the width of the upwelling zone of the stratospheric residual mean circulation, on the order of 2° within a 30° latitude belt, would be consistent with a ~6% decrease in upwelling rate for a fixed total mass flux. In contrast, *Abalos et al*. [2015] find evidence for a strengthening in tropical upwelling throughout the 100–10 hPa layer, based on an evaluation of the residual mean circulation in three reanalyses over a longer time period, from 1979 to 2012. Although there is a large spread in trends between the analyses and between the different methods used to derive upwelling rates, they estimate a range of 2–5%/decade for the increase in $\overline{w^*}$. One difficulty in using reanalyses for deriving trends arises from impacts of changes in the quality and coverage of assimilated observations [e.g., *Iwasaki et al*., 2009]; nevertheless, an increasing trend of this magnitude is consistent with chemistry-climate model simulations [*Garcia and Randel*, 2008; *Butchart et al*., 2010]. On the other hand, *Aschmann et al*. [2014] analyzed chemistry-transport model simulations for the period

between 1980 and 2013 and found that strengthening in tropical upwelling between 70 and 30 hPa ceased around 2002 and actually weakened between 2002 and 2013. Their results could partly explain the apparent inconsistency between our implied decreasing trend for the period of 2004–2014 and any increasing trends derived from longer-term reanalysis data sets.

Figure 9 summarizes the relative contributions of the QBO, seasonal cycles, and ENSO interannual variations to the observed total variance in vertical velocities. At each altitude level or altitude region, the variances associated with these phenomena were determined from the regressed time series of zonal wind shear, annual sinusoids, and MEI, respectively, and divided by the total variance of the time mean velocities shown in Figure 3. In the case of annual sinusoids, it can be shown that the variance is given by the squared amplitude divided by 2. Correlations with the QBO and annual modes are very weak at the lowest altitude level near 17 km, presumably due to increased noise and uncertainty at this close proximity to the tape head, and this level is not shown. Similarly, regressions above about 26 km are not reliable for this kind of variance analysis.

As noted previously, the QBO is found to dominate the total variance in vertical velocity at all levels above about 19 km. Its relative influence increases from being negligible at 18 km to nearly 50% at 22 km. In contrast, the annual mode contributes between 10 and 15% to the total variance, and its relative influence does not vary systematically with height. The amplitudes of both the QBO and seasonal cycle do increase with height above 20 km, but their fractional contributions to the total variance shown here are relatively constant because the total variance also increases monotonically with height above 20 km (Figure 3). Effects due to ENSO, averaged over the altitude region between about 19.5 and 23 km, contribute a little over 5% to the total variance in $\overline{w^*}$. Our results for the ENSO influence on upwelling are in good agreement with the common aspects of ENSO effects seen in the reanalyses examined by *Abalos et al.* [2015], but our QBO contribution is 30–50% larger and the annual cycle contribution is about a factor of 2 smaller. As discussed above, annual amplitudes are likely to be underestimated in a $\overline{w^*}$ time series derived from slices through a seasonal tape recorder signal.

6. Conclusions

We analyzed the upward propagating signals in H_2O and CO mixing ratios measured by MLS in the tropical lower stratosphere (±15° latitude) to construct a ~10 year time series of the residual mean vertical velocity, which at low latitudes, constitutes the main upward branch of the advective component of the Brewer-Dobson circulation. Time mean velocities calculated from H_2O and CO are in good agreement with each other and with values from radiative heating calculations between 20 and 22 km. Below 19 km, the agreement is much poorer and this highlights the difficulty in deriving reliable velocity estimates from tape recorder signals that are in close proximity to the recording heads. The tape recorder based velocities are generally smaller than indicated by ground-based wind profilers, but it is important to note that our values represent tropical means and are thus unable to describe any local or regional-scale spatial variability in upwelling that might be important for direct comparisons. For H_2O, the tape recorder signals are clear enough that a time series of upwelling can be derived with ~2 km vertical resolution and 3–4 month temporal resolution. The CO time series is considerably noisier and cannot be used for a reliable temporal analysis using the sliced window correlation technique.

Vertical velocities are modulated primarily by QBO and annual variations. It is interesting to note that both of these modes are intimately related to atmospheric wave phenomena. The QBO is driven by vertically propagating gravity waves in the tropics, with local feedbacks between the waves and the background zonal wind [*Lindzen and Holton*, 1968], whereas the annual cycle in the deep circulation branch above 70 hPa is driven largely by seasonal forcing from extratropical Rossby and gravity waves [*Haynes et al.*, 1991]. The dissipation of these extratropical waves in the stratosphere controls the downward mass flux at high latitudes, and by mass continuity, affects the upward component of the BDC at low latitudes.

The QBO is found to be the dominant mode of variability in vertical velocities above 19 km, where upward speeds are anticorrelated with the zonal wind shear. The amplitudes of these QBO variations (20–35% of the mean value) grow larger with increasing height, and the slopes of vertical velocities versus zonal wind shear become more negative with increasing height. The latter result is consistent with the decrease in

radiative relaxation time with increasing height in the stratosphere. Our results provide quantitative observational confirmation of QBO-driven meridional circulation anomalies outlined by *Plumb and Bell* [1982], independent of any assumptions associated with radiative heating calculations or fluid dynamical modeling.

Observed annual cycles in vertical velocities show maxima during the months of November–December, and seasonal amplitudes (10–15%) are less than half those of the QBO above 20 km. Below 19 km, the annual mode dominates the total variance. Seasonal amplitudes are likely to be underestimated due to the apparent time resolution (3–4 months) in derived velocities; however, it is unlikely that the true seasonal amplitudes are as large as the observed QBO amplitudes above 20 km altitude. This time resolution limitation is directly related to the 1 year period of the tape heads for H_2O and CO. Higher time resolution could be achieved by applying a Hann window of narrower width for the correlation analysis, but useful results could only be obtained with tape signal periodicities of less than a year, e.g., with signals arising from a semiannually driven trace gas variation.

Interannual anomalies show variability on the order of 5 to 10% and are close to the limit of significance given the level of precision in derived vertical velocities. A major part of the interannual signal is correlated with both ENSO and tropical mean OLR, suggesting an important role by ENSO-driven wave dynamics, or by clouds on lower stratospheric radiative heating, or some combination of the two effects. A small downward trend is seen in mean vertical velocities over the ~9 year record; however, the magnitude of this trend is (0.0014 cm/s/decade or ~6%/decade) is not much larger than the mean uncertainty in derived velocities, and results may be heavily influenced by ENSO variations near beginning and end of the data record. Analysis of a longer time series, such as a merged satellite climatologies [*Froidevaux et al*., 2015] or measurement/model data sets [*Hegglin et al*., 2014], may provide further insight into the interannual variability and possible trends in mean vertical velocities.

Our analysis underscores the value of continuous measurements of water vapor in the tropical lower stratosphere as a tool for monitoring variability and trends in the strength of the BDC. This is in addition to the importance of stratospheric water vapor as a greenhouse gas that contributes to the radiative forcing of climate [e.g., *Forster and Shine*, 1999] and to the role played by stratospheric H_2O in the photochemistry of ozone and other trace gases [e.g., *Shimazaki*, 1985]. It should be pointed out that temporal continuity, spatial coverage, and vertical resolution play a more important role than absolute accuracy or stability of measurements used for analyzing tape recorder signals, in contrast to radiative forcing or photochemical mechanisms that depend directly on the absolute amount of stratospheric water vapor.

Acknowledgments

MLS v3.3 data are available from the NASA Goddard Space Flight Center Earth Sciences (GES) Data and Information Services Center. Zonal wind data were provided by the Institute for Meteorology at Freie Universität Berlin from their Web site at http://www.geo.fu-berlin.de/en/met/ag/strat/produkte/qbo/. MEI and interpolated OLR data provided by the NOAA/OAR/ESRL PSD, Boulder, Colorado, USA, from their Web site at http://www.esrl.noaa.gov/psd. We thank T. Janice Shen for the assistance with the radiative transfer calculations. This work is partly performed at the Jet Propulsion Laboratory, California Institute of Technology sponsored by NASA. The authors acknowledge funding support by the NASA ROSES AST and NEWS programs, and we are grateful for the time and effort of three anonymous referees, who provided exceptionally useful comments and suggestions for this paper.

References

Abalos, M., B. Legras, F. Ploeger, and W. J. Randel (2015), Evaluating the advective Brewer-Dobson circulation in three reanalyses for the period 1979–2012, *J. Geophys. Res. Atmos.*, *120*, 7534–7554, doi:10.1002/2015JD023182.

Andrews, D. G. (2010), *An Introduction to Atmospheric Physics*, 2nd ed., 248 pp., Cambridge Univ. Press, New York, N. Y.

Andrews, D. G., J. R. Holton, and C. B. Leovy (1987), *Middle Atmosphere Dynamics*, 489 pp., Academic, New York, N. Y.

Angell, J. K., and J. Korshover (1962), The biennial wind and temperature oscillation of the equatorial stratosphere and their possible extension to higher latitudes, *Mon. Weather Rev.*, *90*, 127–132.

Aschmann, J., J. P. Burrows, C. Gebhardt, A. Rozanov, R. Hommel, M. Weber, and A. M. Thompson (2014), On the hiatus in the acceleration of tropical upwelling since the beginning of the 21st century, *Atmos. Chem. Phys.*, *14*, 12,803–12,817, doi:10.5194/acp-14-12803-2014.

Austin, J., and F. Li (2006), On the relationship between the strength of the Brewer–Dobson circulation and the age of stratospheric air, *Geophys. Res. Lett.*, *33*, L17807, doi:10.1029/2006GL026867.

Austin, R. T., A. J. Heymsfield, and G. L. Stephens (2009), Retrieval of ice cloud microphysical parameters using the CloudSat millimeter-wave radar and temperature, *J. Geophys. Res.*, *114*, D00A23, doi:10.1029/2008JD010049.

Avallone, L. M., and M. J. Prather (1996), Photochemical evolution of ozone in the lower tropical stratosphere, *J. Geophys. Res.*, *101*, 1457–1461.

Baldwin, M. P., et al. (2001), The quasi-biennial oscillation, *Rev. Geophys.*, *39*, 179–229.

Birner, T., and H. Bönisch (2011), Residual circulation trajectories and transit times into the extratropical lowermost stratosphere, *Atmos. Chem. Phys.*, *11*, 817–827, doi:10.5194/acp-11-817-2011.

Birner, T., S. M. Davis, and D. J. Seidel (2014), The changing width of Earth's tropical belt, *Phys. Today*, *67*(12), 38–44.

Bowman, K. P. (1989), Global patterns of the quasi-biennial oscillation in total ozone, *J. Atmos. Sci.*, *46*, 3328–3343.

Brewer, A. W. (1949), Evidence for a world circulation provided by the measurements of helium and water vapour distribution in the stratosphere, *Q. J. R. Meteorol. Soc.*, *75*, 351–363.

Butchart, N., and A. A. Scaife (2001), Removal of chlorofluorocarbons by increased mass exchange between the stratosphere and troposphere in a changing climate, *Nature*, *410*, 799–802.

Butchart, N., et al. (2010), Chemistry-climate model simulations of twenty-first century stratospheric climate and circulation changes, *J. Clim.*, *23*, 5349–5374, doi:10.1175/2010JCLI3404.1.

Calvo, N., R. R. Garcia, W. J. Randel, and D. Marsh (2010), Dynamical mechanism for the increase in tropical upwelling in the lowermost tropical stratosphere during warm ENSO events, *J. Atmos. Sci.*, *67*, 2331–2340.

Davis, N. A., and T. Birner (2013), Seasonal to multidecadal variability of the width of the tropical belt, *J. Geophys. Res. Atmos.*, *118*, 7773–7787, doi:10.1002/jgrd.50610.
Davis, S. M., and K. H. Rosenlof (2012), A multidiagnostic intercomparison of tropical-width time series using reanalyses and satellite observations, *J. Clim.*, *25*, 1061–1078, doi:10.1175/JCLI-D-11-00127.1.
Dessler, A. E., K. Minschwaner, E. M. Weinstock, E. J. Hintsa, J. G. Anderson, and J. M. Russell III (1996), The effects of tropical cirrus clouds on the abundance of lower stratospheric ozone, *J. Atmos. Chem.*, *23*, 209–220.
Dobson, G. M. B. (1956), Origin and distribution of the polyatomic molecules in the atmosphere, *Proc. R. Soc. A*, *236*, 187–193.
Ehhalt, D. H., F. Rohrer, D. R. Blake, D. E. Kinnison, and P. Konopka (2007), On the use of nonmethane hydrocarbons for the determination of age spectra in the lower stratosphere, *J. Geophys. Res.*, *112*, D12208, doi:10.1029/2006JD007686.
Engel, A., M. Strunk, M. Müller, H.-P. Haase, C. Poss, I. Levin, and U. Schmidt (2002), Temporal development of total chlorine in the highlatitude stratosphere based on reference distributions of mean age derived from CO_2 and SF_6, *J. Geophys. Res.*, *107*(D12), 4136, doi:10.1029/2001JD000584.
Flury, T., D. L. Wu, and W. G. Read (2013), Variability in the speed of the Brewer–Dobson circulation as observed by Aura/MLS, *Atmos. Chem. Phys.*, *13*, 4563–4575, doi:10.5194/acp-13-4563-2013.
Forster, P. M. D., and K. P. Shine (1999), Stratospheric water vapour changes as a possible contributor to observed stratospheric cooling, *Geophys. Res. Lett.*, *26*, 3309–3312.
Froidevaux, L., et al. (2008), Validation of Aura Microwave Limb Sounder stratospheric ozone measurements, *J. Geophys. Res.*, *113*, D15S20, doi:10.1029/2007JD008771.
Froidevaux, L., et al. (2015), Global OZone Chemistry And Related trace gas Data records for the Stratosphere (GOZCARDS): Methodology and sample results with a focus on HCl, H_2O, and O_3, *Atmos. Chem. Phys.*, *15*, 10,471–10,507, doi:10.5194/acp-15-10471-2015.
Fu, Q., and K. N. Liou (1993), Parameterization of the radiative properties of cirrus clouds, *J. Atmos. Sci.*, *50*, 2008–2025.
Fueglistaler, S., and Q. Fu (2006), Impact of clouds on radiative heating rates in the tropical lower stratosphere, *J. Geophys. Res.*, *111*, D23202, doi:10.1029/2006JD007273.
Gage, K. S., J. R. McAfee, D. A. Carter, W. L. Ecklund, A. C. Riddle, G. C. Reid, and B. B. Balsley (1991), Long-term mean vertical motion over the tropical Pacific: Wind-profiling Doppler radar measurements, *Science*, *254*, 1771–1773.
Garća-Herrera, R., N. Calvo, R. R. Garcia, and M. A. Giorgetta (2006), Propagation of ENSO temperature signals into the middle atmosphere: A comparison of two general circulation models and ERA-40 reanalysis data, *J. Geophys. Res.*, *111*, D06101, doi:10.1029/2005JD006061.
Garcia, R., and W. Randel (2008), Acceleration of the Brewer-Dobson circulation due to increases in greenhouse gases, *J. Atmos. Sci.*, *65*, 2731–2739.
Garny, H., T. Birner, H. Bönisch, and F. Bunzel (2014), The effects of mixing on age of air, *J. Geophys. Res. Atmos.*, *119*, 7015–7034, doi:10.1002/2013JD021417.
Gettelman, A., P. H. Lauritzen, M. Park, and J. E. Kay (2009), Processes regulating short-lived species in the tropical tropopause layer, *J. Geophys. Res.*, *114*, D13303, doi:10.1029/2009JD011785.
Harris, F. J. (1978), On the use of windows for harmonic analysis with the discrete Fourier transform, *Proc. IEEE*, *66*, 51, doi:10.1109/PROC.1978.10837.
Haynes, P. H., C. J. Marks, M. E. McIntyre, T. G. Shepherd, and K. P. Shine (1991), On the "downward control" of extratropical diabatic circulations by eddy-induced mean zonal forces, *J. Atmos. Sci.*, *48*, 651–678.
Hegglin, M. I., et al. (2014), Vertical structure of stratospheric water vapour trends derived from merged satellite data, *Nat. Geosci.*, *7*(10), 768–776, doi:10.1038/ngeo2236.
Holton, J. R., and R. S. Lindzen (1972), An updated theory for the quasi-biennial cycle of the tropical stratosphere, *J. Atmos. Sci.*, *29*, 1076–1080.
Holton, J. R., and H.-C. Tan (1980), The influence of the equatorial quasi-biennial oscillation on the global circulation at 50 mb, *J. Atmos. Sci.*, *37*, 2200–2208.
Holton, J. R., P. H. Haynes, M. E. McIntyre, A. R. Douglass, R. B. Rood, and L. Pfister (1995), Stratosphere–troposphere exchange, *Rev. Geophys.*, *33*, 403–439.
Iwasaki, T., H. Hamada, and K. Miyazaki (2009), Comparisons of Brewer-Dobson Circulations diagnosed from reanalyses, *J. Meteorol. Soc. Jpn.*, *87*(6), 997–1006, doi:10.2151/jmsj.87.997.
Jagannadha Rao, V. V. M., M. Venkat Ratnam, and D. Narayana Rao (2002), Study of mean vertical motions over Gadanki (13.5°N, 79.2°E), a tropical station, using Indian MST radar, *Radio Sci.*, *37*(6), 1108, doi:10.1029/2001RS002505.
Jagannadha Rao, V. V. M., D. Rao, N. Rao, M. Venkat Ratnam, K. Mohan, and S. V. B. Rao (2003), Mean vertical velocities measured by Indian MST radar and comparison with indirectly computed values, *J. Appl. Meteorol.*, *42*, 541–552.
Jiang, J. H., B. Wang, K. Goya, K. Hocke, S. D. Eckermann, J. Ma, D. L. Wu, and W. G. Read (2004), Geographical distribution and inter-seasonal variability of tropical deep convection: UARS MLS observations and analyses, *J. Geophys. Res.*, *109*, D03111, doi:10.1029/2003JD003756.
Jiang, J. H., H. Su, C. Zhai, L. Wu, K. Minschewaner, A. Molod, and A. Tompkins (2015), An assessment of upper-troposphere and lower-stratosphere water vapor in GEOS5, MERRA, and ECMWF analysis and reanalyses using Aura MLS observations, *J. Geophys. Res. Atmos.*, *120*, 11,468–11,485, doi:10.1002/2015JD023752.
Kerr-Munslow, A. M., and W. A. Norton (2006), Tropical wave driving of the annual cycle in tropical tropopause temperatures. Part I: ECMWF analyses, *J. Atmos. Sci.*, *63*, 1410–1419.
Kim, J.-E., and M. J. Alexander (2013), A new wave scheme for trajectory simulations of stratospheric water vapor, *Geophys. Res. Lett.*, *40*, 5286–5290, doi:10.1002/grl.50963.
Konopka, P., F. Ploeger, M. Tao, T. Birner, and M. Riese (2015), Hemispheric asymmetries and seasonality of mean age of air in the lower stratosphere: Deep versus shallow branch of the Brewer-Dobson circulation, *J. Geophys. Res. Atmos.*, *120*, 2053–2066, doi:10.1002/2014JD022429.
L'Ecuyer, T. S., and J. H. Jiang (2010), Touring the atmosphere aboard the A-Train, *Phys. Today*, *63*(7), 36–41, doi:10.1063/1.3463626.
Liebmann, B., and C. A. Smith (1996), Description of a complete (interpolated) outgoing longwave radiation dataset, *Bull. Am. Meteorol. Soc.*, *77*, 1275–1277.
Lindzen, R. S., and J. R. Holton (1968), A theory of the quasi-biennial oscillation, *J. Atmos. Sci.*, *25*, 1095–1107.
Livesey, N. J., et al. (2008), Validation of Aura Microwave Limb Sounder O_3 and CO observations in the upper troposphere and lower stratosphere, *J. Geophys. Res.*, *113*, D15S02, doi:10.1029/2007JD008805.
Livesey, N. J., et al. (2011), EOS Aura MLS Version 3.3 Level 2 data quality and description document, *Tech. Rep. D-33509*, Jet Propul. Lab., Calif. Inst. of Technol.
Marsh, D. R., and R. R. Garcia (2007), Attribution of decadal variability in lower-stratospheric tropical ozone, *Geophys. Res. Lett.*, *34*, L21807, doi:10.1029/2007GL030935.

McFarquhar, G. M., and A. J. Heymsfield (1997), Parameterization of tropical cirrus ice crystal size distributions and implications radiative transfer: Results from CEPEX, *J. Atmos. Sci.*, *54*, 2187–2200.
McIntyre, M., and T. Palmer (1984), The "surf zone" in the stratosphere, *J. Atmos. Terr. Phys.*, *46*(9), 825–849.
Minschwaner, K., A. E. Dessler, J. W. Elkins, C. M. Volk, D. W. Fahey, M. Loewenstein, J. R. Podolske, A. E. Roche, and K. R. Chan (1996), Bulk properties of isentropic mixing into the tropics in the lower stratosphere, *J. Geophys. Res.*, *101*, 9433–9439.
Mote, P. W., K. H. Rosenlof, M. E. Mcintyre, E. S. Carr, J. C. Gille, J. R. Holton, J. S. Kinnersley, H. C. Pumphrey, J. M. Russell III, and J. W. Waters (1996), An atmospheric tape recorder: The imprint of tropical tropopause temperatures on stratospheric water vapor, *J. Geophys. Res.*, *101*, 3989–4006.
Mote, P. W., T. J. Dunkerton, M. E. McIntyre, E. A. Ray, P. H. Haynes, and J. M. Russell III (1998), Vertical velocity, vertical diffusion and dilution by midlatitude air in the tropical lower stratosphere, *J. Geophys. Res.*, *103*, 8651–8666, doi:10.1029/98JD00203.
Naujokat, B. (1986), An update of the observed quasi-biennial oscillation of the stratospheric winds over the tropics, *J. Atmos. Sci.*, *43*, 1873–1877.
Newman, P. A., and J. E. Rosenfield (1997), Stratospheric thermal damping times, *Geophys. Res. Lett.*, *24*, 433–436.
Niwano, M., K. Yamazaki, and M. Shiotani (2003), Seasonal and QBO variations of ascent rate in the tropical lower stratosphere as inferred from UARS HALOE trace gas data, *J. Geophys. Res.*, *108*(D24), 4794, doi:10.1029/2003JD003871.
Olaguer, E. P., H. Yang, and K. K. Tung (1992), A reexamination of the radiative balance of the stratosphere, *J. Atmos. Sci.*, *49*, 1242–1263.
Olsen, E. T., S. Granger, E. Manning, and J. Blaisdell (2007), AIRS/AMSU/HSB Version 5 Level 3 Quick Start. [Available at http://airs.jpl.nasa.gov/AskAirs.]
Oppenheim, A. V., R. W. Schafer, and J. R. Buck (1999), *Discrete-Time Signal Processing*, 468 pp., Prentice Hall, Upper Saddle River, N. J.
Plumb, R. A., and R. C. Bell (1982), A model of the quasi-biennial oscillation on an equatorial beta-plane, *Q. J. R. Meteorol. Soc.*, *108*, 335–352.
Plumb, R. A., and J. Eluszkiewicz (1999), The Brewer–Dobson circulation: Dynamics of the tropical upwelling, *J. Atmos. Sci.*, *56*, 868–890.
Randel, W., J. Gille, A. Roche, J. Kumer, J. Mergenthaler, J. Waters, E. Fishbein, and W. Lahoz (1993), Stratospheric transport from the tropics to middle latitudes by planetary-wave mixing, *Nature*, *365*, 533–535.
Randel, W. J., F. Wu, R. Swinbank, J. Nash, and A. O'Neill (1999), Global QBO circulation derived from UKMO stratospheric analyses, *J. Atmos. Sci.*, *56*, 457–474.
Randel, W. J., R. R. Garcia, and F. Wu (2002), Time-dependent upwelling in the tropical lower stratosphere estimated from the zonal-mean momentum budget, *J. Atmos. Sci.*, *59*, 2141–2152.
Randel, W. J., R. R. Garcia, and F. Wu (2008), Dynamical balances and tropical stratospheric upwelling, *J. Atmos. Sci.*, *65*, 3584–3595.
Read, W. G., et al. (2007), Aura Microwave Limb Sounder upper tropospheric and lower stratospheric H_2O and relative humidity with respect to ice validation, *J. Geophys. Res.*, *112*, D24S35, doi:10.1029/2007JD008752.
Reed, R. J., W. J. Campbell, L. A. Rasmussen, and D. G. Rodgers (1961), Evidence of downward-propagating annual wind reversal in the equatorial stratosphere, *J. Geophys. Res.*, *66*, 813–818.
Rosenlof, K. H. (1995), Seasonal cycle of the residual mean meridional circulation in the stratosphere, *J. Geophys. Res.*, *100*, 5173–5191.
Rosenlof, K. H., and J. R. Holton (1993), Estimates of the stratospheric residual circulation using the downward control principle, *J. Geophys. Res.*, *98*, 10,465–10,479.
Schoeberl, M. R., B. N. Duncan, A. R. Douglass, J. Waters, N. Livesey, W. Read, and M. Filipiak (2006), The carbon monoxide tape recorder, *Geophys. Res. Lett.*, *33*, L12811, doi:10.1029/2006GL026178.
Schoeberl, M. R., A. R. Douglass, R. S. Stolarski, S. Pawson, S. E. Strahan, and W. Read (2008), Comparison of lower stratospheric tropical mean vertical velocities, *J. Geophys. Res.*, *113*, D24109, doi:10.1029/2008JD010221.
Schwartz, M. J., et al. (2008), Validation of the Aura Microwave Limb Sounder temperature and geopotential height measurements, *J. Geophys. Res.*, *113*, D15S11, doi:10.1029/2007JD008783.
Shimazaki, T. (1985), *Minor Constituents in the Middle Atmosphere*, 443 pp., Terra Sci., Tokyo.
Solomon, S., J. T. Kiehl, R. R. Garcia, and W. Grose (1986), Tracer transport by the diabatic circulation deduced from satellite observations, *J. Atmos. Sci.*, *43*, 1603–1617.
Su, H., and J. H. Jiang (2013), Tropical clouds and circulation changes during the 2006-07 and 2009-10 El Niños, *J. Clim.*, *26*, 399–413, doi:10.1175/JCLI-D-12-00152.1.
Su, H., J. H. Jiang, G. L. Stephens, D. G. Vane, and N. J. Livesey (2009), Radiative effects of upper tropospheric clouds observed by Aura MLS and CloudSat, *Geophys. Res. Lett.*, *36*, L09815, doi:10.1029/2009GL037173.
Wallace, J. M. (1973), General circulation of the tropical lower stratosphere, *Rev. Geophys.*, *11*, 191–222.
Waugh, D. W., and T. M. Hall (2002), Age of stratospheric air: Theory, observations and models, *Rev. Geophys.*, *40*(4), 1010, doi:10.1029/2000RG000101.
World Meteorological Organization (2011), Scientific assessment of ozone depletion: 2010, *Global Ozone Res. and Monitor. Proj. Rep. 52*, 511 pp., World Meteorol. Organ.
Wolter, K., and M. S. Timlin (2011), El Niño/Southern Oscillation behaviour since 1871 as diagnosed in an extended multivariate ENSO index (MEI.ext), *Int. J. Climatol.*, *31*, 1074–1087.
Wu, D. L., J. H. Jiang, W. G. Read, R. T. Austin, C. P. Davis, A. Lambert, G. L. Stephens, D. G. Vane, and J. W. Waters (2008), Validation of the Aura MLS cloud ice water content measurements, *J. Geophys. Res.*, *113*, D15S10, doi:10.1029/2007JD008931.